

Disentanglement with Factor Quantized Variational Autoencoders

Gulcin Baykal^{a,b,*}, Melih Kandemir^b, Gozde Unal^c

^a*Department of Computer Engineering, Istanbul Technical University, Istanbul, Türkiye*

^b*Department of Mathematics and Computer Science, University of Southern Denmark, Odense, Denmark*

^c*Department of AI and Data Engineering, Istanbul Technical University, Istanbul, Türkiye*

Abstract

Disentangled representation learning aims to represent the underlying generative factors of a dataset in a latent representation independently of one another. In our work, we propose a discrete variational autoencoder (VAE) based model where the ground truth information about the generative factors are not provided to the model. We demonstrate the advantages of learning discrete representations over learning continuous representations in facilitating disentanglement. Furthermore, we propose incorporating an inductive bias into the model to further enhance disentanglement. Precisely, we propose scalar quantization of the latent variables in a latent representation with scalar values from a global codebook, and we add a total correlation term to the optimization as an inductive bias. Our method called FactorQVAE is the first method that combines optimization based disentanglement approaches with discrete representation learning, and it outperforms the former disentanglement methods in terms of two disentanglement metrics (DCI and InfoMEC) while improving the reconstruction performance. Our code can be found at <https://github.com/ituvisionlab/FactorQVAE>.

Keywords: Disentanglement, Discrete Representation Learning, Vector Quantized Variational Autoencoders

1. Introduction

Discovering and extracting meaningful representations from raw data relevant to the task at hand has been the main purpose of representation learning. While the answer to the fundamental question of *what makes a representation good* varies based on the task to perform, one possible answer is being "disentangled" [1]. A disentangled representation depicts the distinct and independent underlying generative factors of the data in its different, interpretable components. As

*Corresponding author

Email addresses: baykalg@itu.edu.tr (Gulcin Baykal), kandemir@imada.sdu.dk (Melih Kandemir), gozde.unal@itu.edu.tr (Gozde Unal)

an example from the image modality, a disentangled representation captures the underlying generative factors such as object color, shape, orientation, or lighting, with its separate dimensions.

Disentangled representations advance performance in numerous unlike domains and tasks such as biometrics [2], fairness in representations [3], human motion prediction [4], and image manipulation [5]. Despite its contributions to various domains, unsupervised disentanglement has proven to be challenging, and even impossible, without certain restrictive assumptions [6]. Disentangled representation learning can be considered as an ill-posed problem as there is no unique way to disentangle the generative factors in data [7]. Lack of knowledge about the true generative factors for most of the datasets makes it more difficult to obtain and evaluate disentangled representations. Therefore, the success of disentangled representation learning heavily relies on the inductive biases deployed into the model. Disentanglement may be induced via architecture design [8], restrictive constraints used as regularizers [9], and enhanced loss functions [10].

A recent work proposes QLAE [11], a VAE based model that uses discrete representations as a better inductive bias for disentanglement. Discrete representation learning has gained further importance with the tremendous success of vector quantization for representation learning [12], and been used in recent large generative models like LDM [13] and DALL-E [14]. While the discrete representations are better suited for expressing categories that shape the observation space [12], Hsu et al. [11] use this rationale for disentanglement, and quantize the continuous representations with a small set of scalar values in order to force the model to assign constant meaning to each value. For each dimension of the representation, Hsu et al. [11] define a separate set of scalar values, referred to as a codebook, and quantize each value using a scalar from its corresponding codebook. The quantizing value is selected based on its proximity to the corresponding variable in the continuous representation. Although Hsu et al. [11] demonstrate that using individual codebooks for each dimension, rather than a single global codebook, improves disentanglement, we identify certain challenges with this approach.

In QLAE, the quantization of each latent variable is restricted with its own codebook that includes a predefined number of scalar values, \mathbf{k} . Assume two generative factors, *shape* and *orientation* that are ideally captured with different latent variables. These factors have a different number of options, \mathbf{n} and \mathbf{m} where $\mathbf{n} < \mathbf{m}$, respectively. Therefore, the range of values in the latent representation may vary in order to capture these options, such that the range of latent values for *orientation* might be wider since $\mathbf{n} < \mathbf{m}$. Quantizing the latent values of different generative factors using individual codebooks can be limiting in terms of representation capacity. For example, using \mathbf{k} scalars may be insufficient to represent \mathbf{m} possible *orientations*, while at the same time, \mathbf{k} could be excessive for representing \mathbf{n} possible *shapes*. Instead of this restrictive design, a model with a single, global codebook can be designed such that disentanglement is further encouraged with regularizers rather than individual codebooks. Furthermore, this model can learn to assign distinct partitions of the global codebook to

different generative factors for a better representation capability.

In this work, we design a novel framework that uses discrete representation learning for disentanglement with a single, global codebook. Different than QLAE, we incorporate further inductive biases to aid disentanglement, and introduce a "total correlation" term to the optimization. As detailed in Section 2, various regularizers have been proposed to enhance disentanglement, with total correlation being one such regularizer. This term modifies the original loss function by adding a penalty that encourages disentangled representations, thereby improving the overall disentanglement of the model [15]. We summarize our contributions as follows:

- We introduce FactorQVAE that originally combines factorization as a regularizer and the discrete VAEs for disentanglement.
- We report the effects of factorization and discretization on disentanglement individually and demonstrate the effectiveness of their novel combination for improved disentangled representations.
- We redesign the training frameworks of two discrete VAE models, VQ-VAE [12] and dVAE [14], to enhance disentanglement and evaluate their performance.

In our work, we compare FactorQVAE with recent and state-of-the-art disentanglement models using three different datasets and two different disentanglement evaluation metrics. We demonstrate that our model performs close to or better than the other methods in terms of disentanglement.

2. Related Work

Disentangled Representation Learning: Methods for disentangled representation learning can be categorized by their model types, supervision levels, and independence assumptions [16]. We choose the VAE as the base model architecture over alternatives such as generative adversarial networks (GAN) [17] and diffusion model [18]. Several VAE-based approaches have been proposed for disentanglement, incorporating various assumptions and regularizers. For example, Higgins et al. [19] introduce a penalty coefficient, β , to the loss component in VAE that affects disentanglement; Kim and Mnih [15] include a total correlation term to enforce disentanglement during optimization; Chen et al. [10] decompose the VAE loss component affecting disentanglement into multiple parts and assign different coefficients to these parts, rather than using a single β coefficient, in order to improve disentanglement without sacrificing reconstruction quality; Whittington et al. [9] add biologically inspired activity constraints during training; and Hsu et al. [11] utilize discrete representations to aid in disentanglement.

In terms of supervision, since unsupervised disentanglement is theoretically impossible without inductive biases [6], weakly-supervised [20] and self-supervised

[21] methods have also been proposed for disentanglement. While all the aforementioned methods generally assume statistical independence between the generative factors and the variables in the latent representation, some approaches also consider causal relationships between the generative factors [22].

In our work, we propose an unsupervised VAE-based method that assumes independent generative factors and innovatively integrates discrete representation learning with regularized optimization to enhance disentanglement.

Discrete Representation Learning: After Oord et al. [12] demonstrated the significant advantages of discrete representation learning, vector quantization, introduced as a discretization method in [12], gained popularity for various representation learning tasks across different modalities, including image generation [23], music generation [24], and text decoding [25].

Vector quantization is also utilized in Wu et al. [26] for object-centric representation learning using multiple codebooks, where each codebook captures a distinct semantic meaning. An object’s representation is then obtained by combining embeddings from these semantic codebooks. The study demonstrates that vector quantization with multiple codebooks aids in disentangling semantic features in object-centric representation learning. In contrast to Wu et al. [26], which relies on the known number of ground truth semantic factors to determine the number of codebooks, our method is unsupervised and specifically designed for disentanglement.

Mercatali and Freitas [27] propose to use discrete VAEs for disentangling the generative factors in natural language. Our method differs from Mercatali and Freitas [27], as their approach requires knowledge of the number of possible values for each generative factor during training, whereas our method is fully unsupervised.

3. Background

3.1. Discrete Variational Autoencoders

Discrete VAEs aim to represent high-dimensional data x using a low dimensional, discrete latent representation z by maximizing the Evidence Lower Bound (ELBO) objective:

$$\mathcal{L}_{\text{ELBO}} = \mathbb{E}_{q(z|x)}[\log p(x|z)] - \text{KL}[q(z|x)||p(z)], \quad (1)$$

where the generative model $p(x|z)$ is implemented as a decoder, the approximated posterior $q(z|x)$ is implemented as an encoder, and $p(z)$ is the prior. This objective addresses the challenge of approximating the posterior distribution $p(z|x)$, which is intractable due to the complexity of computing $p(x)$. Variational inference is used to approximate this posterior with a tractable distribution $q(z|x)$ and optimize the ELBO, making $q(z|x)$ as close as possible to the true posterior.

In discrete VAEs, the d -dimensional latent variables z are sampled from a Categorical distribution as $z \sim \text{Cat}(z|\pi)$. The encoder outputs unnormalized log probabilities $l = [l_1, \dots, l_d]$, and the probability masses π of this Categorical

distribution are obtained as $\text{softmax}(l)$. Subsequently, z are fed into the decoder to reconstruct x .

VQVAE [12] is a discrete VAE variant featuring a learnable codebook $\mathcal{M} \in \mathbb{R}^{K \times C}$ composed of K number of C -dimensional embeddings, which is trained to represent a dataset. In VQVAE, an observation x is represented by the selected embeddings from \mathcal{M} . At first, the continuous latent representation $z_e(x) = \mathcal{E}_\theta(x)$ where $z_e(x) \in \mathbb{R}^{N \times N \times C}$ is obtained by the encoder \mathcal{E}_θ . Then, the Euclidean distances between $z_e(x)$ and the embeddings in \mathcal{M} are calculated. The discrete latent variables $z \in \mathbb{R}^{N \times N \times K}$ are sampled as one-hot from the posterior $q(z|x)$. The deterministic posterior Categorical distribution is defined as follows:

$$q(z = k|x) = \begin{cases} 1 & \text{if } k = \text{argmin}_j \|z_e(x)_i - e_j\|_2 \\ 0 & \text{otherwise} \end{cases} \quad (2)$$

where $k, j \in \{1, \dots, K\}$, $i \in 1, \dots, N \times N$, $z_e(x)_i$ is the i^{th} embedding in $z_e(x)$, and e_j is the j^{th} codebook embedding. The discrete latent variables z are used to retrieve the corresponding embeddings from \mathcal{M} obtaining the quantized representation $z_q(x)$ through matrix multiplication, $z_q(x) = z * \mathcal{M}$. Finally, $z_q(x) \in \mathbb{R}^{N \times N \times C}$ is fed into the decoder \mathcal{D}_ϕ , and $x = \mathcal{D}_\phi(z_q(x))$ is obtained.

While VQVAE’s encoder learns a continuous representation to be directly quantized with the codebook \mathcal{M} based on the distances, another discrete VAE variant dVAE [14]’s encoder outputs $z_e(x) \in \mathbb{R}^{N \times N \times K}$ that is treated as the unnormalized log probabilities l of a Categorical distribution over K number of embeddings in \mathcal{M} , and $z \sim \text{Cat}(z|\text{softmax}(l))$ is attained. Instead of feeding the discrete latent variables z to the decoder directly, they are used to retrieve the corresponding codebook embeddings to construct $z_q(x)$ as in VQVAE.

In our work, we investigate the performance of both dVAE and VQVAE in terms of disentanglement and incorporate our method into both to further enhance disentanglement.

3.2. Disentangled Representation Learning

Assume that the observation x sampled from the generative model $p(x|z)$ has the underlying generative factors $\mathbf{s} = (s_1, \dots, s_F)$, and the factorized density $p(z) = \prod_{i=1}^d p(z_i)$ holds for z . Disentanglement is the process of learning to represent F number of mutually independent underlying generative factors \mathbf{s} where $p(\mathbf{s}) = \prod_{j=1}^F p(s_j)$ holds, in the separate, independent d number of components of the latent representation z . Single latent variables should capture changes in a specific underlying factor, while remaining relatively unaffected by changes in other factors [1].

In our work, we seek for a model that can achieve $\mathcal{D}_\phi(\mathcal{E}_\theta(x)) \sim x$ with a high degree of disentanglement.

3.3. Disentanglement Metrics

Disentanglement metrics can be categorized as *intervention-based*, *predictor-based*, and *information-based* [28]. Intervention-based metrics evaluate disentanglement by fixing factors, creating subsets of data points, and comparing

the corresponding codes and factors within these subsets to produce a score. Predictor-based metrics involve training a regressor/classifier f to predict generative factor realizations from latents $f(z) \mapsto s$, followed by analyzing the predictor to assess the usefulness of each latent dimension in accurately predicting the generative factors. Information-based metrics calculate a disentanglement score by estimating the mutual information between the latents and the generative factors.

In our work, we select "Disentanglement, Completeness and Informativeness (DCI)" metric [29] from the predictor-based metrics as they are generally the best performing solutions [28], and "Modularity, Explicitness, and Compactness (InfoMEC)" from the information-based metrics as it is the most up-to-date metric proposed in the literature [11] for evaluation.

3.3.1. DCI

To calculate DCI scores, F number of regressors or classifiers are trained to predict generative factors $\mathbf{s} = (s_1, \dots, s_F)$ from the latent variables z . Assume $f_j(z \mapsto s_j)$ is a predictor mapping z to j^{th} generative factor s_j . An importance matrix $M \in \mathbb{R}^{d \times F}$ can be formed such that M_{ij} is the magnitude of the weight learned by the predictor f_j which indicates the relationship between the i^{th} latent variable z_i and s_j . Here d refers to the number of latent variables.

Disentanglement (D), also known as modularity, refers to the extent to which z separates the generative factors \mathbf{s} , with each latent variable capturing at most one distinct generative factor. D is calculated as follows:

$$\begin{aligned} P_{ij} &= M_{ij} / \sum_{k=0}^{F-1} M_{ik}, \\ D_i &= 1 + \sum_{k=0}^{F-1} P_{ik} \log_F P_{ik}, \\ \rho_i &= \sum_j M_{ij} / \sum_{ij} M_{ij}, \\ D &= \sum_i \rho_i D_i, \end{aligned}$$

where P_{ij} represents z_i 's probability of being important for predicting each s_j , D_i is the disentanglement score for z_i , and ρ_i is the weight of D_i for average disentanglement score D .

Completeness (C), also known as compactness, refers to the extent to which each generative factor s_j is captured by a single latent variable. C is calculated as follows:

$$\begin{aligned} \tilde{P}_{ij} &= M_{ij} / \sum_{k=0}^{d-1} M_{kj}, \\ C_j &= 1 + \sum_{k=0}^{d-1} \tilde{P}_{kj} \log_d \tilde{P}_{kj}, \\ \rho_j &= \sum_i M_{ij} / \sum_{ij} M_{ij}, \\ C &= \sum_j \rho_j C_j, \end{aligned}$$

where \tilde{P}_{ij} represents each z_i 's probability of being important for predicting s_j , C_i is the completeness score for s_j , and ρ_j is the weight of C_j for average completeness score C .

Informativeness (I), also known as explicitness, is the extent to which z captures information about the underlying generative factors \mathbf{s} . I is calculated as the mean accuracies of F different predictors that are essentially learning the relationship between z and \mathbf{s} .

3.3.2. InfoMEC

Instead of training predictors and using their weights and accuracies to evaluate disentanglement, mutual information (MI) between z_i and s_j can be used as a notion of informativeness. MI quantifies the amount of information shared between the latent variable z_i and the underlying factor s_j , providing a clear and objective metric for how well z_i captures s_j . By focusing on MI, we can assess disentanglement in terms of how effectively each latent variable encodes distinct factors of variation, without the need for potentially biased or indirect measures from predictor performance. MI between z_i and s_j can be defined as:

$$\begin{aligned} I(z_i; s_j) &= D_{\text{KL}}(p(s_j, z_i) \| p(s_j)p(z_i)) \\ &= H(s_j) - H(s_j | z_i), \end{aligned}$$

where $H(\cdot)$ is the entropy function. Normalized mutual information (NMI) which depicts the relationship between z and \mathbf{s} as a matrix can be defined as:

$$\text{NMI}(z_i, s_j) = \frac{I(z_i, s_j)}{H(s_j)}.$$

To compute the modularity of z_i , Chen et al. [10] propose to use the gap between the two largest elements in the i^{th} row of NMI, while Hsu et al. [11] prefer using the ratio of the largest element in the i^{th} row to the row sum, and propose InfoM as the average modularity which is defined as:

$$\text{InfoM} = \left(\frac{1}{d} \sum_{i=1}^d \frac{\max_j \text{NMI}_{ij}}{\sum_{j=1}^F \text{NMI}_{ij}} - \frac{1}{F} \right) / \left(1 - \frac{1}{F} \right).$$

To compute the average compactness, Hsu et al. [11] propose InfoC which is defined as:

$$\text{InfoC} = \left(\frac{1}{F} \sum_{j=1}^F \frac{\max_i \text{NMI}_{ij}}{\sum_{i=1}^d \text{NMI}_{ij}} - \frac{1}{d} \right) / \left(1 - \frac{1}{d} \right).$$

To compute explicitness, Hsu et al. [11] borrow the framework of predictive \mathcal{V} -information [30], and follows these steps:

$$\begin{aligned}
H_{\mathcal{V}}(s_j|z) &= \inf_{f \in \mathcal{V}} \mathbb{E}_{s \sim p(s), z \sim p(z|s)} [-\log p(s_j|f(z))], \\
H_{\mathcal{V}}(s_j|\emptyset) &= \inf_{f \in \mathcal{V}} \mathbb{E}_{s \sim p(s)} [-\log p(s_j|f(\emptyset))], \\
I_{\mathcal{V}}(z \rightarrow s_j) &= H_{\mathcal{V}}(s_j|\emptyset) - H_{\mathcal{V}}(s_j|z), \\
\text{NMI}_{\mathcal{V}}(z \rightarrow s_j) &= \frac{I_{\mathcal{V}}(z \rightarrow s_j)}{H_{\mathcal{V}}(s_j|\emptyset)}, \\
\text{InfoE} &= \frac{1}{F} \sum_{j=1}^F \text{NMI}_{\mathcal{V}}(z \rightarrow s_j),
\end{aligned}$$

where \mathcal{V} is an allowable function class for the computation of information, $H_{\mathcal{V}}(s_j|z)$ is the predictive conditional \mathcal{V} -entropy, $H_{\mathcal{V}}(s_j|\emptyset)$ is the marginal \mathcal{V} -entropy, $I_{\mathcal{V}}(z \rightarrow s_j)$ is the predictive \mathcal{V} -information of s_j , $\text{NMI}_{\mathcal{V}}(z \rightarrow s_j)$ is the normalized predictive \mathcal{V} -information, and InfoE is the average explicitness.

In our work, we follow the literature and set $d > F$. Specifically, we set $d = 2 * F$ where F changes based on the dataset. As a consequence of this inequality, achieving both perfect disentanglement (modularity) and perfect completeness (compactness) is impossible. Therefore, achieving a better disentanglement (modularity) value is prioritized.

4. Method

The overview of our method FactorQVAE is shown in Figure 1. In FactorQVAE, we originally integrate discrete representation learning with factorization for enhanced disentanglement. While we use a single sample in the first stage to explain discrete representation learning (Figure 1-yellow highlighted background), we prefer batch view to explain factorization better (Figure 1-pink highlighted background).

We start by making key adjustments to the vector quantization process described in Section 3.1 in order to tailor it for disentanglement. Referring to Figure 1, we view the output of \mathcal{E}_{θ_1} as a feature tensor depicting spatial information about input x , and further transform the features by nonlinear operations \mathcal{E}_{θ_2} to obtain a vector latent representation $z_e(x) \in \mathbb{R}^{d * C \times 1}$. Hence, $z_e(x)$ now captures the underlying generative factors with its latent variables, rather than spatial information.

Originally, VQVAE quantizes the C dimensional vectors in $z_e(x)$ with the embeddings in the codebook \mathcal{M} with a deterministic choice based on the distances. Instead of vector quantization, we propose scalar latent variable quantization with a single, global codebook $\mathcal{M} \in \mathbb{R}^{K \times 1}$ consisting K number of scalar values, and name this model QVAE, rather than VQVAE. Consequently, the output of \mathcal{E}_{θ_1} which is an $N \times N \times C$ dimensional feature tensor is transformed into $z_e(x) \in \mathbb{R}^{d \times 1}$ so that each latent variable in $z_e(x)$ can be quantized with a scalar from \mathcal{M} .

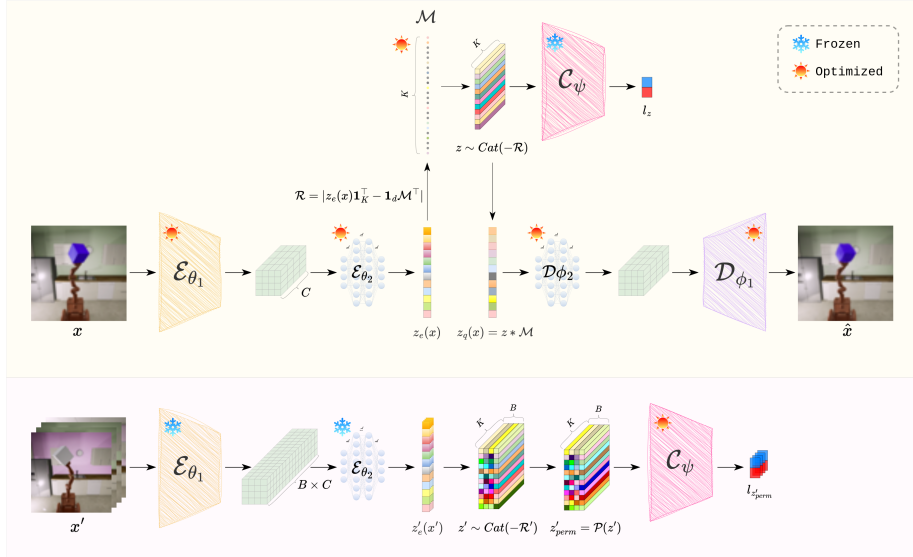


Figure 1: At the first stage (yellow background), an input x is encoded into a latent representation $z_e(x)$ by the encoder \mathcal{E}_{θ_1} , followed by some nonlinear operations \mathcal{E}_{θ_2} . Each latent variable in $z_e(x)$ is quantized with the colored scalars from the codebook \mathcal{M} whose indices z are sampled based on the distances \mathcal{R} between $z_e(x)$ and \mathcal{M} . The quantized latent representation $z_q(x)$ is transformed by nonlinear operations \mathcal{D}_{ϕ_2} , and fed into the decoder \mathcal{D}_{ϕ_1} to reconstruct x . The discriminator \mathcal{C}_{ψ} outputs log probabilities that its input is sampled from $q(z)$ rather than from $\bar{q}(z)$. At second stage (pink background), a new data batch x' is sampled. Permuter \mathcal{P} permutes the one-hot indices z' across the latent dimensions, and yields z'_{perm} (best viewed in PDF with zoom).

We hypothesize that using a lower dimensional latent representation $z_e(x) \in \mathbb{R}^{d \times 1}$ and quantizing scalar latent variables, rather than using a higher dimensional latent representation $z_e(x) \in \mathbb{R}^{d \times C \times 1}$ and quantizing embeddings in the latent, can better maintain a balance between reconstruction and disentanglement performance. This is because a higher dimensional latent representation, quantized with the embeddings from a codebook, has a higher information capacity. This increased capacity may shift the emphasis towards improving reconstruction performance during training, potentially compromising disentanglement performance. Therefore, we proceed with scalar quantization in the proposed method.

Apart from the representation design, we further modify the variational family. Rather than using a deterministic categorical posterior as in Equation 2, we define a stochastic categorical posterior proposed by Sønderby et al. [31] as:

$$\mathcal{R} = |z_e(x)\mathbf{1}_K^\top - \mathbf{1}_d \mathcal{M}^\top|, \quad (3)$$

$$q(z|x) = \text{Cat}(-\mathcal{R}). \quad (4)$$

In Equation 3, we calculate the distance matrix $\mathcal{R} \in \mathbb{R}^{d \times K}$ between $z_e(x) \in \mathbb{R}^{d \times 1}$ and \mathcal{M} . We use $\mathbf{1}_K$ and $\mathbf{1}_d$ vectors of ones with K and d dimensions, respectively,

for computational ease in calculation of the distance matrix \mathcal{R} . \mathcal{R} holds i^{th} latent variable's distances to \mathcal{M} in its i^{th} row.

Since the closest scalar in \mathcal{M} has the lowest distance, we use $-\mathcal{R}$ as the parameters of the Categorical distribution to be able to sample the closest scalar with a higher probability in Equation 4. Sampling from the stochastic posterior $q(z|x)$ yields the discrete variables $z \in \mathbb{R}^{d \times K}$ which are essentially the one-hot representations of the indices of the quantizing scalars for d number of latent variables. Since sampling from a Categorical distribution is not a differentiable operation in the traditional sense that hurts end-to-end training, we use Gumbel-Softmax distribution for a differentiable approximation to categorical sampling [32, 33]. These differentiable samples will be essential when we add the total correlation term to the optimization.

The quantized representation $z_q(x) \in \mathbb{R}^{d \times 1}$ is obtained by a matrix multiplication of the discrete variables z and \mathcal{M} . $z_q(x)$ is originally fed into the decoder \mathcal{D}_{ϕ_1} in VQVAE as it is the quantization of the feature tensor. In our case, we further transform the latent vector $z_q(x)$ into a feature tensor by nonlinear layers in \mathcal{D}_{ϕ_2} before feeding it into \mathcal{D}_{ϕ_1} to reconstruct input x .

Although FactorQVAE is first built upon a VQVAE based method, the dVAE framework can be also used as the discrete representation learning part of our model. While \mathcal{R} in Equation 3 is calculated to define the parameters of the Categorical distribution in FactorQVAE, we can directly learn these parameters by \mathcal{E}_θ as in dVAE. Based on dVAE, we can learn $z_e(x) \in \mathbb{R}^{d \times K}$ which essentially represents the parameters of the Categorical distribution over each codebook element for each latent dimension, and perform $z \sim \text{Cat}(z_e(x))$. We explore the importance of the design of the discrete representation learning module by modeling FactordVAE based on dVAE, along with FactorQVAE.

We have covered the discrete representation learning aspect of the framework in the first stage. Next, we explain how we add factorization to the training as a regularizer that enforces disentanglement. As suggested by Kim and Mnih [15], a new term called "total correlation" can be incorporated into the ELBO, which is then maximized over the overall loss:

$$\begin{aligned} \mathcal{L}(\mathcal{M}, \theta_1, \theta_2, \phi_1, \phi_2) = & \frac{1}{N} \sum_{i=1}^N [\mathbb{E}_{q(z|x^i)} [\log p(x^i|z)] - \beta \text{KL}(q(z|x^i)||p(z))] \\ & - \gamma \text{KL}(q(z)||\bar{q}(z)), \end{aligned} \quad (5)$$

where the total correlation term is given by $\text{KL}(q(z)||\bar{q}(z))$. Here, $q(z) = \frac{1}{N} \sum_{i=1}^N q(z|x^i)$ is the marginal posterior over the entire dataset, and $\bar{q}(z) = \prod_{j=1}^d q(z_j)$ indicates factorial distribution. The total correlation term encourages the marginal posterior to factorize, thereby promoting disentanglement.

Since the total correlation calculations are intractable, a common approach is to resort to a practical solution to approximate the total correlation [15]. First, sampling from $q(z)$ is performed by sampling from $q(z|x_B^i)$ where x_B^i is a sample within the randomly selected batch B . For approximating $\bar{q}(z)$, we can sample a new batch B' and sample $z' \sim q(z|x_{B'}^i)$, then randomly permute

across the batch for each latent dimension by the permutation operator \mathcal{P} to obtain $z'_{perm} = \mathcal{P}(z')$. This permutation operation is visually exemplified in Figure 1 in the second stage. It is important to note that in FactorQVAE, each latent dimension consists of K dimensional one-hot vectors unlike FactorVAE [15] where each latent dimension is one dimensional.

Essentially, by permuting the samples across each latent dimension independently, we create a new set of samples that behave as if each dimension z_j was independently sampled from $q(z_j)$. This independence and matching distribution are exactly what $\bar{q}(z)$ represents, and thus the distribution of the permuted batch z'_{perm} approximates $\bar{q}(z)$ when the batch size is sufficiently large.

We minimize the KL divergence between $q(z)$ and $\bar{q}(z)$ using the density ratio trick:

$$\text{KL}(q(z)||\bar{q}(z)) = \mathbb{E}_{q(z)} \left[\log \frac{q(z)}{\bar{q}(z)} \right], \quad (6)$$

$$\approx \mathbb{E}_{q(z)} \left[\log \frac{\mathcal{C}_\psi(z)}{1 - \mathcal{C}_\psi(z)} \right], \quad (7)$$

where \mathcal{C}_ψ is a discriminator that approximates the density ratio in Equation 6. Assume $\mathcal{C}_\psi(z)$ is the estimated probability that z are sampled from $q(z)$ rather than $\bar{q}(z)$. In order to train such a discriminator that can differentiate between the samples from $q(z)$ and $\bar{q}(z)$, \mathcal{C}_ψ should be optimized by minimizing the following loss function:

$$\mathcal{L}(\psi) = \mathbb{E}_{z \sim q(z)} [\log(\mathcal{C}_\psi(z))] + \mathbb{E}_{z'_{perm} \sim \bar{q}(z)} [\log(1 - \mathcal{C}_\psi(z'_{perm}))]. \quad (8)$$

The second stage in Figure 1 shows the training procedure of \mathcal{C}_ψ . As we need to backpropagate the gradients from \mathcal{C}_ψ to the other modules, z must remain differentiable, which is ensured by our design. Algorithm 1 presents the pseudocode of the overall FactorQVAE training that we propose.

5. Experiments

5.1. Experimental Settings

We conduct our experiments on three datasets: Shapes3D [34], Isaac3D [35], and MPI3D [36]. Each dataset corresponds to simple, medium, hard complexity, respectively. Further details about the datasets are given in Appendix A.1.

We choose recent and state-of-the-art disentanglement models to compare our model: β -VAE [19], FactorVAE [15], BioAE [9], and QLAE [11]. We also evaluate autoencoder (AE), QVAE which is the scalar quantizing version of VQVAE [12] instead of vector quantization, and dVAE [14]. We use the same network architecture across all baseline models to ensure a fair comparison. While this may result in minor deviations from the original findings reported in the literature, these differences are not significant enough to impact the overall conclusions. Further details like the network architecture and hyperparameter selection for each model are given in Appendix A.3.

Algorithm 1 Training algorithm of FactorQVAE

Input: Observations $(\mathbf{x}_{\text{train}}^i)_{i=1}^N$, batch size B , β , γ , optimizers g_1 and g_2
Initialize the network parameters $\theta_1^{[0]}, \theta_2^{[0]}, \phi_1^{[0]}, \phi_2^{[0]}, \psi^{[0]}$, the codebook $\mathcal{M}^{[0]}$,
temperature parameter $\tau^{[0]}$, learning rates $\alpha_1^{[0]}$ for g_1 and $\alpha_2^{[0]}$ for g_2 .
for $t = 1, 2, \dots, T$ **do**
 $x \leftarrow$ Random minibatch from $\mathbf{x}_{\text{train}}$ of size B
 $z_e(x) \leftarrow \mathcal{E}_{\theta_2^{[t-1]}} \left(\mathcal{E}_{\theta_1^{[t-1]}}(x) \right)$
 $\mathcal{R} \leftarrow |z_e(x) \mathbf{1}_K^\top - \mathbf{1}_d \mathcal{M}^{[t-1]\top}|$
 $z \sim \text{RelaxedOneHotCategorical}(\text{temperature} = \tau^{[t-1]}, \text{logits} = -\mathcal{R})$
 $\mathcal{L}_1 \leftarrow \frac{1}{B} \sum_{i \in B} \left[-\log p(x^i | z^i) + \beta \text{KL}(q(z^i | x^i) \| p(z)) \right] + \gamma \log \frac{\mathcal{C}_{\psi^{[t-1]}(z^i)}}{1 - \mathcal{C}_{\psi^{[t-1]}(z^i)}}$
 $\mathcal{M}^{[t]}, \theta_1^{[t]}, \theta_2^{[t]}, \phi_1^{[t]}, \phi_2^{[t]} \leftarrow g_1(\nabla_{\mathcal{M}, \theta_1, \theta_2, \phi_1, \phi_2} \mathcal{L}_1, \text{learning rate} = \alpha_1^{[t-1]})$
 $x' \leftarrow$ Random minibatch from $\mathbf{x}_{\text{train}}$ of size B
 $z'_e(x') \leftarrow \mathcal{E}_{\theta_2^{[t]}} \left(\mathcal{E}_{\theta_1^{[t]}}(x') \right)$
 $\mathcal{R}' \leftarrow |z'_e(x') \mathbf{1}_K^\top - \mathbf{1}_d \mathcal{M}^{[t]\top}|$
 $z' \sim \text{RelaxedOneHotCategorical}(\text{temperature} = \tau^{[t-1]}, \text{logits} = -\mathcal{R}')$
 $z'_{\text{perm}} \leftarrow \mathcal{P}(z')$
 $\mathcal{L}_2 \leftarrow \frac{1}{2B} \sum_{i \in B} \left[\log \mathcal{C}_{\psi^{[t-1]}(z^i)} + \log(1 - \mathcal{C}_{\psi^{[t-1]}(z'_{\text{perm}}{}^i)}) \right]$
 $\psi^{[t]} \leftarrow g_2(\nabla_{\psi} \mathcal{L}_2, \text{learning rate} = \alpha_2^{[t-1]})$
 $\tau^{[t]} \leftarrow \text{CosineAnneal}(\tau^{[t-1]}, t)$
 $\alpha_1^{[t]} \leftarrow \text{CosineAnneal}(\alpha_1^{[t-1]}, t)$
 $\alpha_2^{[t]} \leftarrow \text{CosineAnneal}(\alpha_2^{[t-1]}, t)$
end for

5.2. Discussions

We conduct various experiments to analyze the effects of discrete representation learning and factorization separately. We detail the results of selecting discrete representation learning over continuous representation learning, QVAE over dVAE, scalar quantization over vector quantization, and a global codebook over codebooks per latent dimension in this section.

To evaluate the disentanglement numerically, we use DCI and InfoMEC, with details provided in Section 3.3. Table 1 shows both DCI and InfoMEC results of the models for all datasets. As disentanglement should be obtained along with acceptable reconstruction performance, we further present the mean squared error (MSE) of the models in Table 1.

For the visual evaluation of disentanglement and reconstruction performance, we intervene on the latent variables separately, and decode it to the image space to see if only a single generative factor is affected without artifacts in the image.

Figure 2 compares FactorQVAE with its closest alternative, QLAE, on Shapes3D. While QLAE still struggles with image reconstruction artifacts, FactorQVAE produces cleaner results. Additionally, QLAE’s outputs are more

Table 1: Evaluation of models across all datasets for disentanglement (DCI and InfoMEC) and reconstruction ($\text{MSE} \times 10^4$) performance.

model	D \uparrow	I \uparrow	C \uparrow	InfoM \uparrow	InfoE \uparrow	InfoC \uparrow	MSE \downarrow
Shapes3D							
AE	0.52	0.82	0.42	0.55	0.99	0.41	0.3
β -VAE	0.56	0.89	0.65	0.62	0.76	0.75	1.6
FactorVAE	0.72	0.94	0.79	0.61	0.81	0.86	1.6
BioAE	0.41	0.75	0.32	0.52	0.99	0.33	1.1
QLAE	0.91	1.00	0.75	0.71	0.99	0.54	0.9
dVAE	0.89	0.95	0.71	0.70	0.99	0.45	4.4
QVAE	0.73	0.94	0.54	0.69	0.93	0.38	0.8
FactorVAE (ours)	0.91	0.95	0.70	0.49	0.99	0.32	4.7
FactorQVAE (ours)	0.86	0.97	0.65	0.84	0.89	0.52	0.6
Isaac3D							
AE	0.22	0.75	0.18	0.39	0.61	0.15	0.2
β -VAE	0.45	0.80	0.58	0.49	0.46	0.53	1.5
FactorVAE	0.51	0.80	0.64	0.56	0.47	0.62	1.6
BioAE	0.29	0.78	0.23	0.40	0.57	0.17	0.8
QLAE	0.57	0.89	0.48	0.52	0.65	0.37	0.5
dVAE	0.53	0.80	0.45	0.60	0.62	0.33	3.6
QVAE	0.56	0.81	0.49	0.51	0.72	0.34	0.4
FactorVAE (ours)	0.62	0.78	0.56	0.86	0.66	0.56	5.7
FactorQVAE (ours)	0.59	0.75	0.56	0.68	0.64	0.45	0.7
MPI3D							
AE	0.10	0.57	0.10	0.30	0.25	0.11	0.5
β -VAE	0.36	0.70	0.42	0.39	0.35	0.39	1.2
FactorVAE	0.20	0.61	0.31	0.40	0.23	0.32	1.4
BioAE	0.23	0.66	0.26	0.28	0.37	0.24	0.9
QLAE	0.36	0.76	0.41	0.31	0.40	0.38	0.6
dVAE	0.33	0.67	0.31	0.39	0.66	0.23	2.2
QVAE	0.34	0.61	0.31	0.31	0.77	0.27	0.9
FactorVAE (ours)	0.29	0.56	0.23	0.37	0.60	0.25	4.4
FactorQVAE (ours)	0.46	0.67	0.44	0.33	0.94	0.36	1.1

entangled, as seen in the 8th row, where *orientation* and *shape* are intertwined. Although FactorQVAE shows fewer artifacts and greater disentanglement, some values for generative factors are still missing. For instance, in the 6th and 12th rows, *orange* is absent from the *floor color*, suggesting that a generative factor’s value still depends on the semantic information from other factors. This highlights the ongoing challenge of achieving full disentanglement, even with a simpler dataset. Figure 3 compares the results of FactorQVAE and FactorVAE on the Isaac3D dataset. FactorQVAE produces cleaner reconstructions with fewer artifacts and shows more consistent disentanglement. In FactorVAE, we observe that changing some latent variables affects multiple generative factors, whereas FactorQVAE exhibits more stable and independent control of the latent variables. Figure 4 present the image reconstruction results after latent traversals for MPI3D datasets. While we observe that FactorQVAE and the other models yield better disentanglement for Shapes3D and Isaac3D datasets in Figure 2 and Figure 3, respectively, Figure 4 clearly demonstrates the challenges of disentangling MPI3D dataset for both β -VAE and FactorQVAE. Therefore, we observe that there is still a long way to achieve an acceptable level of disentanglement in challenging environments.

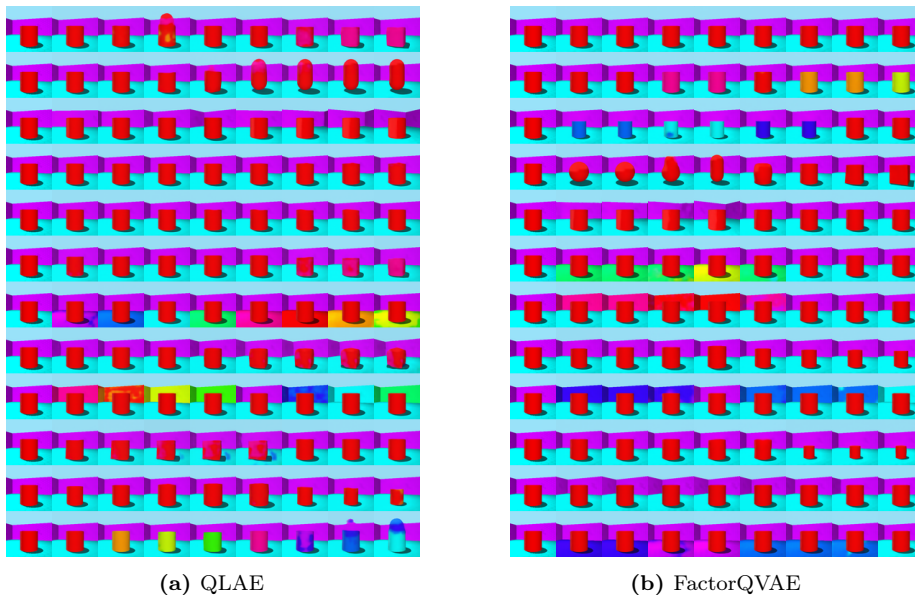


Figure 2: Latent traversal on the same image with QLAE and FactorQVAE for Shapes3D dataset. Each row i shows the result of manipulating the i^{th} latent. For QLAE, the i^{th} latent is intervened on with a linear interpolation between the minimum and maximum values in the corresponding i^{th} codebook while it is intervened on with a linear interpolation between the minimum and maximum values in the global codebook for FactorQVAE.

Figure 5 presents the heatmaps of NMI matrices used in InfoMEC calculation for Shapes3D, and Figure 6 and Figure 7 present the heatmaps of the information matrices used in DCI calculation for Isaac3D and MPI3D, respectively. As we use different disentanglement metrics DCI and InfoMEC, we visually showcase how they are calculated. Figure 5 and Figure 6 clearly demonstrate the relationship between the latent variables and the generative sources, with FactorQVAE appearing to balance disentanglement and completeness better than the other models. On the other hand, Figure 7 visually demonstrates the failure of all models in capturing all the generative factors in a challenging dataset like MPI3D. Still, FactorQVAE seems to be capturing more factors in a disentangled manner.

We conduct an additional experiment on the Shapes3D dataset, where we swap the latent variables of two images individually. Figure 8 presents the results of this latent variable swapping for QLAE and FactorQVAE, using two pairs of images. \mathbf{z} column shows the original images, and the \mathbf{z}_i column displays the results after swapping the i^{th} latent variables. QLAE shows poor reconstruction performance, with noticeable artifacts, particularly for latent variables \mathbf{z}_0 and \mathbf{z}_9 , which do not correspond to a single generative factor (see Figure 5 for the relationship between latent variables and generative sources). In contrast, FactorQVAE successfully transfers the generative factor values between images without introducing artifacts.

For the first image pair, the generative factors are swapped exactly between

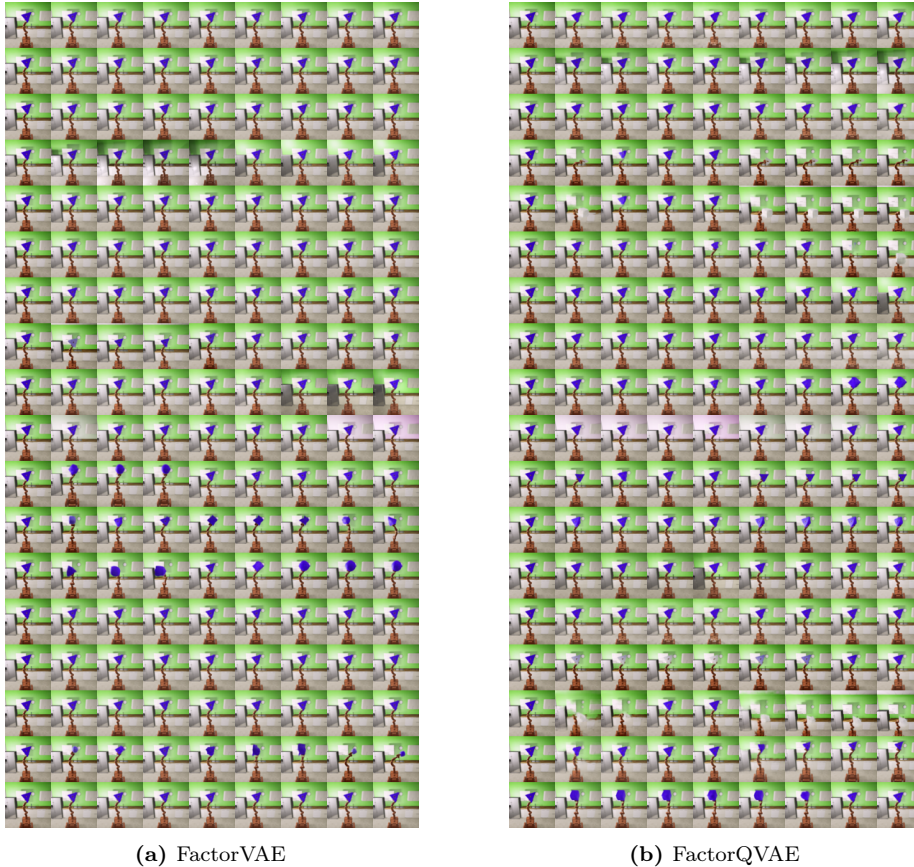


Figure 3: Latent traversal on the same image with FactorVAE and FactorQVAE for Isaac3D dataset. Each row i shows the result of manipulating the i^{th} latent. For FactorVAE, the i^{th} latent is intervened on with a linear interpolation between "original latent value - 3" and "original latent value + 3" while it is intervened on with a linear interpolation between the minimum and maximum values in the global codebook for FactorQVAE.

the images. However, when multiple latent variables represent the same generative factor, such as \mathbf{z}_5 and \mathbf{z}_{11} for *floor hue*, only one may influence the reconstructions. For the second image pair, the exact values of the generative factors may not transfer perfectly, as seen in the *floor hue* swapping with \mathbf{z}_5 and \mathbf{z}_{11} . This result highlights that, even if a latent variable represents a single generative factor, its effect may still depend on the image’s semantic content.

Discrete vs continuous representation learning: To start with, we compare discrete representation learning and continuous representation learning in terms of disentanglement and reconstruction. When we compare models that learn discrete representations, such as QLAE and QVAE, with models that learn continuous representations, such as β -VAE and FactorVAE, by referring to Table 1, we observe that while the discrete representation learning models

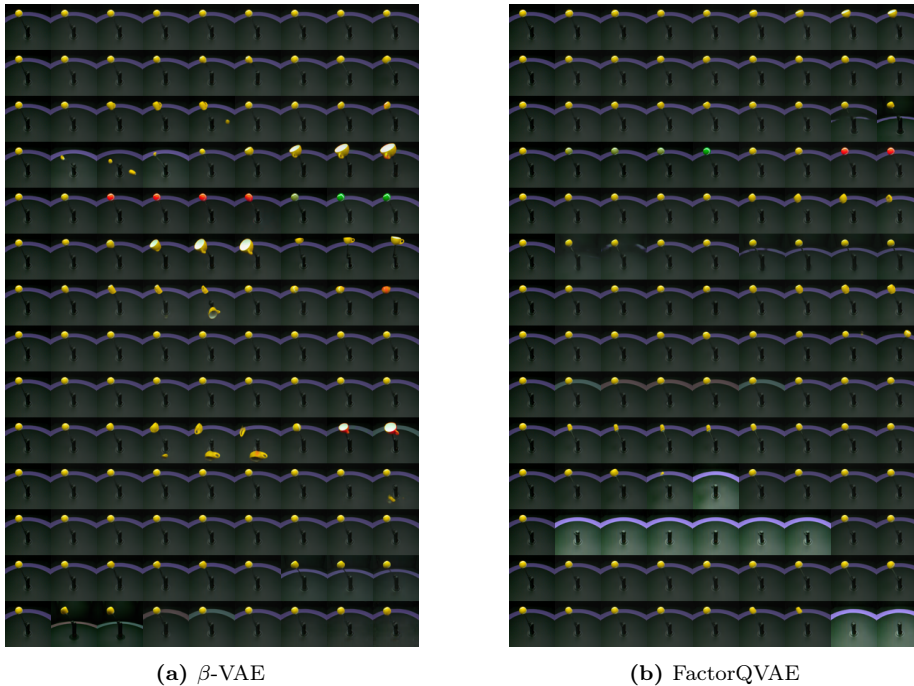


Figure 4: Latent traversal on the same image with β -VAE and FactorQVAE for MPI3D dataset. Each row i shows the result of manipulating the i^{th} latent. For β -VAE, the i^{th} latent is intervened on with a linear interpolation between "original latent value - 3" and "original latent value + 3" while it is intervened on with a linear interpolation between the minimum and maximum values in the global codebook for FactorQVAE.

outperform the continuous representation learning models in terms of the DCI metric for all datasets, they also outperform the latter in terms of InfoMEC in most cases. In addition to disentanglement performance, the discrete representation learning models achieve better reconstruction performance. Since achieving both acceptable reconstruction and disentanglement performance together is difficult, an AE trained solely on the reconstruction objective provides the best reconstruction performance, as expected. However, discrete representation learning models can also achieve reconstruction performance that is acceptably close to that of autoencoders (AE).

QVAE vs dVAE: Although discrete representation learning improves performance, the design of the model remains crucial for this enhancement. Therefore, we implement dVAE and QVAE as the discrete representation learning models, and observe that QVAE leads to more balanced performance between reconstruction and disentanglement. When we go through the disentanglement performance of dVAE and QVAE in Table 1, we see that dVAE outperforms QVAE in most of the settings. However, dVAE cannot achieve adequate reconstruction performance as it seems, which is essential along with disentanglement.

We can view the issue with dVAE as a posterior collapse problem, meaning

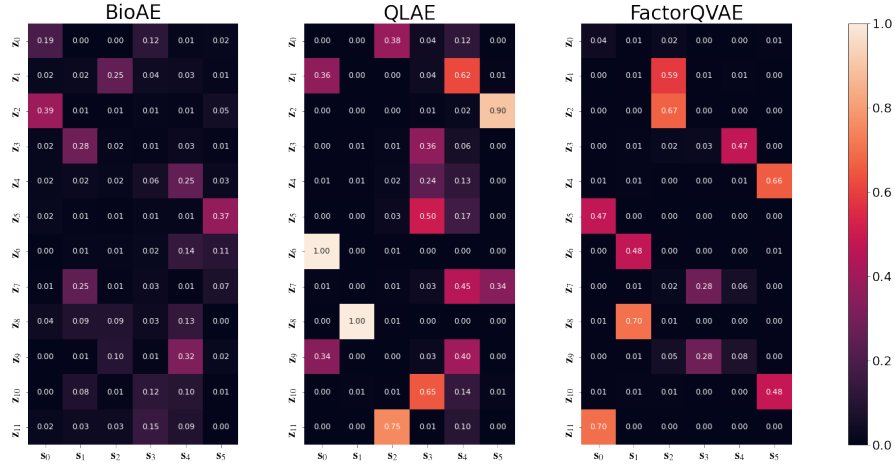


Figure 5: Visualization of the NMI matrix which is used in InfMEC calculation for Shap3D dataset.



Figure 6: Visualization of the information matrices used in DCI calculation for Isaac3D dataset.

that the model prioritizes minimizing the KL term rather than the reconstruction term. As a result, the latent representation fails to sufficiently capture information about the input data, although it achieves better disentanglement. This behavior likely stems from the fact that the parameters of the Categorical distribution are learned by the encoder, which is more challenging to optimize. Consequently, the model finds a shortcut to minimize the loss by focusing on reducing the KL term instead of maintaining a proper balance. Given this performance gap between QVAE and dVAE, we proceed with QVAE.

Effects of factorization: After demonstrating the contribution of discrete representation learning in terms of both disentanglement and reconstruction

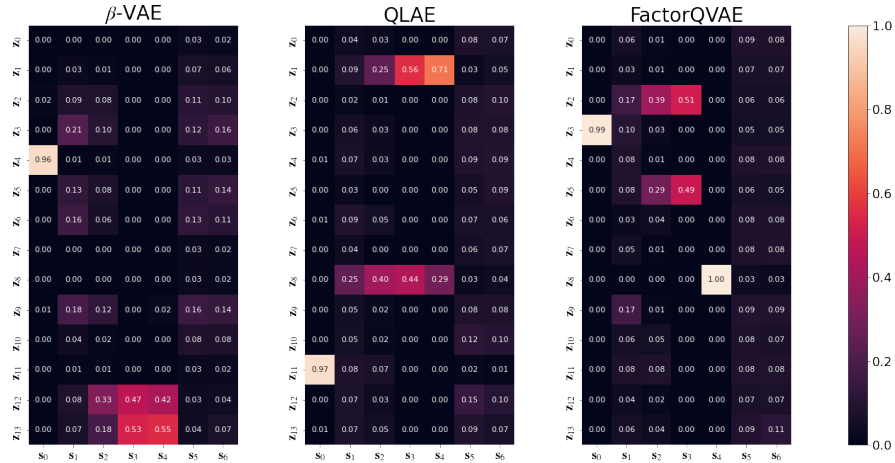


Figure 7: Visualization of the information matrix which is used in DCI calculation for MPI3D dataset.

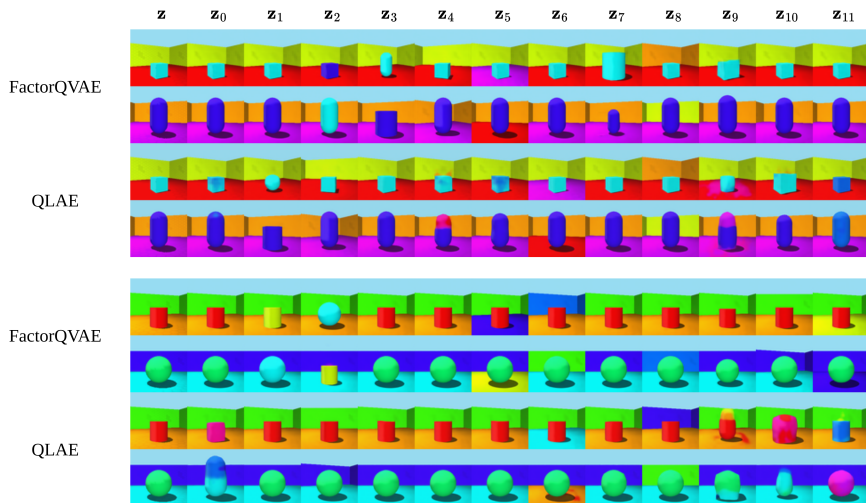


Figure 8: Latent variable swapping between two different images. We select two different pairs of images, and show them in column \mathbf{z} of each image block. For each image block, the first two rows show the latent swapping results for FactorQVAE while the last two rows show the latent swapping results for QLAE. Each \mathbf{z}_i column displays the effects of swapping the i^{th} latent variables between two images.

performance, we incorporate factorization as an inductive bias to further enhance disentanglement. Our model FactorQVAE achieves the best performance in most of the settings for both DCI and InfoMEC as observed in Table 1. As stated in Section 3.3, the disentanglement (D) and its counterpart, modularity

Table 2: Effects of codebook (\mathcal{M}) design using Shapes3D dataset.

\mathcal{M}	D \uparrow	I \uparrow	C \uparrow	InfoM \uparrow	InfoE \uparrow	InfoC \uparrow	MSE \downarrow
(V)QVAE							
32×1	0.69	0.97	0.52	0.75	0.88	0.39	1.4
64×1	0.73	0.94	0.54	0.69	0.93	0.38	0.8
128×1	0.72	0.79	0.64	0.51	0.98	0.41	1.7
64×8	0.68	0.99	0.50	0.52	0.99	0.33	0.6
64×16	0.65	0.99	0.49	0.47	0.99	0.29	0.4
Factor(V)QVAE							
32×1	0.81	0.94	0.66	0.82	0.92	0.57	1.1
64×1	0.86	0.97	0.65	0.84	0.89	0.52	0.6
128×1	0.82	0.91	0.62	0.68	0.97	0.41	1.5
64×8	0.78	0.97	0.63	0.59	0.99	0.48	0.5
64×16	0.75	0.96	0.60	0.51	0.98	0.45	0.4

(InfoM), are prioritized to evaluate the disentanglement in general. We observe that FactorQVAE achieves the best D and InfoM values in most of the settings while it also achieves compatible completeness (compactness) values. Besides, FactorQVAE’s reconstruction performance is on a par with the models having the best reconstruction performance.

We further highlight the FactorVAE results to emphasize on the effects of factorization in continuous representation learning. We present that FactorVAE generally outperforms β -VAE in terms of disentanglement while achieving similar reconstruction performance with the latter. Moreover, FactorVAE achieves the best DCI and InfoMEC scores in some of the settings, demonstrating the effectiveness of factorization. Therefore, combining factorization with discrete representation learning boosts the performance as expected.

Lastly, we observe that factorization also improves the performance of dVAE in terms of disentanglement. Even though FactordVAE achieves the best DCI and InfoMEC scores in some of the settings, FactordVAE is not favorable as a consequence of its poor reconstruction performance.

Scalar quantization vs vector quantization: In order to test our intuition behind scalar quantization explained in Section 4, we form various codebook configurations, and test them using Shapes3D dataset. Table 2 presents the results of our experiments. Firstly, we focus on the effects of scalar quantization. We name the models VQVAE and FactorVQVAE when the codebook \mathcal{M} consists of embeddings, and we perform vector quantization. We observe that going from scalars to embeddings, and further increasing the dimensionality of the embeddings leads to a slightly better reconstruction performance as expected. However, we monitor a notable decrease in disentanglement, especially in terms of InfoMEC. Therefore, we experimentally confirm that scalar quantization leads to better maintain a balance between the reconstruction and disentanglement performance. Moreover, we experience a stability problem when we train VQVAE and FactorVQVAE with $\mathcal{M} \in \mathbb{R}^{64 \times 8}$ and $\mathcal{M} \in \mathbb{R}^{64 \times 8}$ as the training is more vulnerable to changes in β and γ coefficients. Due to its demonstrated benefits, we opted for scalar quantization.

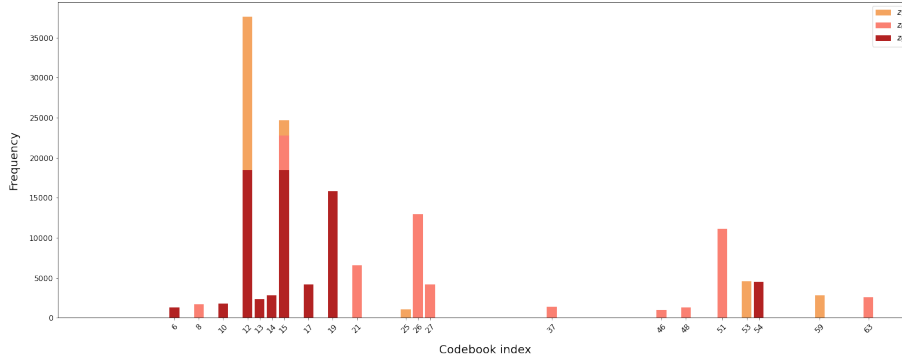


Figure 9: Frequencies of the codebook elements used in specific latent dimensions learned by FactorQVAE in Isaac3D dataset.

Beyond scalar and vector quantization comparison, we look at the effects of number of elements in \mathcal{M} for scalar quantization. We see a slight difference in evaluation metrics when we have different number of elements in \mathcal{M} . That indicates that the performance of both QVAE and FactorQVAE is resistant to number of elements in \mathcal{M} . Therefore, we prefer not to engineer dataset specific values for the number of elements in \mathcal{M} , and proceed with 64 number of scalar values in \mathcal{M} for all datasets.

Global codebook vs codebooks per latent dimensions: The efficiency of using a global codebook instead of codebooks per latent dimensions can be observed to some extent by comparing QVAE with QLAE. Even though QLAE uses a deterministic categorical posterior for each latent variable rather than a stochastic categorical posterior like ours, we can still make sense out of this comparison.

When we look at Table 1, we see that QVAE is on a par with QLAE both for disentanglement and reconstruction performance, which does not highlight the significance of having a global codebook. However, the good side of having a global codebook is that we let the model learn how to partition the latent space. As we exemplify in Section 1, different generative factors might have different number of options. Hence, setting fixed length codebooks per latent might be restrictive in terms of representativeness. To support our intuition, we conduct an experiment on Isaac3D dataset for FactorQVAE. Figure 6 shows that for FactorQVAE, latents z_1 and z_6 capture the generative factor s_6 , while z_9 captures s_8 . As detailed in Section A.1, s_6 is the lighting direction, and it has 6 possible values, while s_8 is wall color, and it has 4 possible values. Based on our intuition, s_6 should be represented with a latent space larger than s_8 's latent space. Thus, we analyze which codebook elements are used in the latent dimensions capturing these generative sources, and their frequencies, in Figure 9. We observe that the number of codebook elements representing s_6 in latent dimensions z_1 and z_6 is greater than the number of codebook elements representing s_8 in z_9 , which aligns with our expectations. We further observe

in Figure 9 that the sets of codebook elements representing different generative factors are mostly disjoint, serving as an evidence that FactorQVAE learns to assign different sets of codebook elements for different generative factors. The overlapping codebook elements for different generative factors capture more information, and are used in various latent dimensions. Even though we still cannot talk about a perfect separation of the codebook, our model provides a promising direction on this matter.

6. Conclusion

The proposed FactorQVAE extends the discrete representation learning model QVAE by introducing a regularizer called factorization to enhance disentanglement in representation learning. First, we show that discrete representation learning is more suitable than continuous representation learning for disentanglement. We further demonstrate that incorporating an inductive bias into a discrete representation learning model improves its performance, with FactorQVAE outperforming previous methods in most settings in terms of both disentanglement and reconstruction.

Although the proposed method improves disentanglement performance, there is still room for improvement in challenging settings, such as real-world environments exemplified by the MPI3D dataset. We observe that neither previous methods nor FactorQVAE achieve an acceptable level of disentangled representation learning in such challenging settings. However, we believe our work can inspire future developments that extend discrete representation learning models to address disentangled representation learning for real-world problems, as we have already demonstrated the effectiveness of discrete representation learning for disentanglement within a factorizable scalar latent space.

Acknowledgment

In this work, Gulcin Baykal was supported by TÜBİTAK 2214-A International Research Fellowship Programme for PhD Students and Google DeepMind Scholarship Program at ITU. Computing resources used during this research were provided by the Scientific Research Project Unit of Istanbul Technical University [project number MOA-2019-42321].

Appendix

A. Further Experimental Details

We use PyTorch Lightning [37] framework in our implementation. All models are trained for 100K iterations on every dataset using a single NVIDIA V100 GPU. We use a batch size of 256 and the Adam optimizer with an initial learning rate of $1e^{-3}$. The learning rate is then annealed following a cosine annealing schedule from $1e^{-3}$ to $1.25e^{-6}$ over the first 50K iterations. We also apply a temperature

Table A.3: Hyperparameters of the best performing models.

model	Shapes3D	Isaac3D	MPI3D
β -VAE	$\beta = 10^{-4}$	$\beta = 5 \times 10^{-5}$	$\beta = 10^{-5}$
FactorVAE	$\beta = 10^{-4}$ $\gamma = 10^{-4}$	$\beta = 5 \times 10^{-5}$ $\gamma = 5 \times 10^{-5}$	$\beta = 10^{-5}$ $\gamma = 10^{-5}$
BioAE	$\beta_{\text{nonneg}} = 1$ $\beta_{\text{activity}} = 10^{-2}$	$\beta_{\text{nonneg}} = 1$ $\beta_{\text{activity}} = 0.1$	$\beta_{\text{nonneg}} = 1$ $\beta_{\text{activity}} = 10^{-2}$
QLAE	$\lambda_{\text{quantize}} = 10^{-2}$ $\lambda_{\text{commit}} = 10^{-2}$ $n_v = 16$	$\lambda_{\text{quantize}} = 10^{-2}$ $\lambda_{\text{commit}} = 10^{-2}$ $n_v = 16$	$\lambda_{\text{quantize}} = 10^{-2}$ $\lambda_{\text{commit}} = 10^{-2}$ $n_v = 16$
dVAE	$\beta = 5 \times 10^{-3}$	$\beta = 10^{-5}$	$\beta = 5 \times 10^{-5}$
QVAE	$\beta = 10^{-3}$	$\beta = 5 \times 10^{-5}$	$\beta = 5 \times 10^{-5}$
FactordVAE	$\beta = 5 \times 10^{-3}$ $\gamma = 5 \times 10^{-4}$	$\beta = 10^{-5}$ $\gamma = 10^{-5}$	$\beta = 5 \times 10^{-5}$ $\gamma = 5 \times 10^{-6}$
FactorQVAE	$\beta = 10^{-3}$ $\gamma = 10^{-4}$	$\beta = 5 \times 10^{-5}$ $\gamma = 5 \times 10^{-5}$	$\beta = 5 \times 10^{-5}$ $\gamma = 10^{-6}$

annealing schedule for the Gumbel-Softmax, defined as $\tau = \exp(-10^{-5} \cdot t)$, where τ represents the temperature and t is the global training step. Model and dataset specific hyperparameters are detailed in Section A.2.

A.1. Datasets

Shapes3D: It is a dataset consisting 480,000 images of various 3D geometric objects. It has 6 generative factors: floor hue, wall hue, object hue, object scale, object shape, and camera orientation having 10, 10, 10, 8, 4, and 15 possible values, respectively.

Isaac3D: It is a dataset consisting 737,280 images of a synthetic robot arm holding objects in different configurations. It has 9 generative factors: object shape, robot’s horizontal axis, robot’s vertical axis, camera height, object scale, lighting intensity, lighting direction, object color, and wall color having 3, 8, 5, 4, 4, 4, 6, 4, and 4 possible values, respectively.

MPI3D: It is a dataset consisting 460,800 images of a real robot arm holding objects in different configurations. It has 7 generative factors: object color, object shape, object size, camera height, background color, robot’s horizontal axis, and robot’s vertical axis having 4, 4, 2, 3, 3, 40, and 40 possible values, respectively.

A.2. Hyperparameters

We run controlled experiments for all models on all datasets, and report the key hyperparameters of the best performing models in Table A.3. We use the same coefficient names from the original papers, and try to stick to original hyperparameter values from them. As the complexities of the datasets vary a lot, we naturally obtain the best performances with different hyperparameters.

Table A.4: Notations of network layers used on all models.

Notation	Description
$\text{Conv}_n^{(3 \times 3)}$	2D Conv layer (out_ch= n , kernel= 3, stride= 1, padding= 1)
Linear_n	Linear layer (out_ch= n)
MaxPool	2D Max pooling layer (kernel_size= 2)
Upsample	2D upsampling layer (scale_factor= 2)
EncResBlock_n	$3 \times (\text{ReLU} \rightarrow \text{Conv}_n^{(3 \times 3)}) \rightarrow \text{ReLU} \rightarrow \text{Conv}_n^{(1 \times 1)} + \text{identity}$
DecResBlock_n	$\text{ReLU} \rightarrow \text{Conv}_n^{(1 \times 1)} \rightarrow 3 \times (\text{ReLU} \rightarrow \text{Conv}_n^{(3 \times 3)}) + \text{identity}$
Dense_n	$\text{ReLU} \rightarrow \text{Linear}_n \rightarrow \text{ReLU} \rightarrow \text{Linear}_n \rightarrow \text{ReLU}$

A.3. Model Description

We use a similar architecture used in [14]. The common building blocks used in the architecture are given in Table A.4. For all datasets, the image size is 64 ($w = h = 64$). We use a codebook $\mathcal{M} \in \mathbb{R}^{64 \times 1}$. Designs of encoding and decoding parts are given as follows:

Encoding: $x \in \mathbb{R}^{w \times h \times 3} \rightarrow \text{Conv}_n^{(3 \times 3)} \rightarrow [\text{EncResBlock}_n]_2 \rightarrow \text{MaxPool} \rightarrow [\text{EncResBlock}_{2*n}]_2 \rightarrow \text{MaxPool} \rightarrow [\text{EncResBlock}_{4*n}]_2 \rightarrow \text{Dense}_m \rightarrow \text{Linear}_o \rightarrow z_e(x) \in \mathbb{R}^{p \times 1}$

Decoding: $z_q(x) \in \mathbb{R}^{d \times 1} \rightarrow \text{Linear}_{w/4 \times h/4 \times 16} \rightarrow [\text{DecResBlock}_{4*n}]_2 \rightarrow \text{UpSample} \rightarrow [\text{DecResBlock}_{2*n}]_2 \rightarrow \text{UpSample} \rightarrow [\text{DecResBlock}_n]_2 \rightarrow \text{ReLU} \rightarrow \text{Conv}_3^{(1 \times 1)} \rightarrow \hat{x} \in \mathbb{R}^{w \times h \times 3}$

$n = 128$, and $m = 128$ for all datasets. For AE, BioAE, QLAE, QVAE, and FactorQVAE, $o = p = d$ where d is the latent dimension. For β -VAE and FactorVAE, x is encoded into a latent representation with $o = 2 \times d$ dimensions for the mean and the variance of the posterior distribution, and $p = d$. For dVAE and FactordVAE, $o = p = d * K$ as the encoding part learns the parameters of a distribution over the codebook elements.

References

- [1] Y. Bengio, A. Courville, P. Vincent, Representation learning: A review and new perspectives, IEEE Trans. Pattern Anal. Mach. Intell. 35 (2013).
- [2] W. Yang, J. Huang, D. Luo, W. Kang, Efficient disentangled representation learning for multi-modal finger biometrics, Pattern Recognition 145 (2024) 109944.
- [3] T. Jang, X. Wang, Fades: Fair disentanglement with sensitive relevance, in: Proceedings of the IEEE/CVF Conference on Computer Vision and Pattern Recognition (CVPR), 2024.
- [4] C. Gu, J. Yu, C. Zhang, Learning disentangled representations for controllable human motion prediction, Pattern Recognition 146 (2024) 109998.

- [5] C. Xiao, Q. Yang, X. Xu, J. Zhang, F. Zhou, C. Zhang, Where you edit is what you get: Text-guided image editing with region-based attention, *Pattern Recognition* 139 (2023) 109458.
- [6] F. Locatello, S. Bauer, M. Lucic, G. Raetsch, S. Gelly, B. Schölkopf, O. Bachem, Challenging common assumptions in the unsupervised learning of disentangled representations, in: *Proceedings of the 36th International Conference on Machine Learning*, 2019.
- [7] D. Horan, E. Richardson, Y. Weiss, When is unsupervised disentanglement possible?, in: *Advances in Neural Information Processing Systems*, 2021.
- [8] F. Leeb, G. Lanzillotta, Y. Annadani, M. Besserve, S. Bauer, B. Schölkopf, Structure by architecture: Structured representations without regularization, in: *International Conference on Learning Representations*, 2023.
- [9] J. C. R. Whittington, W. Dorrell, S. Ganguli, T. Behrens, Disentanglement with biological constraints: A theory of functional cell types, in: *International Conference on Learning Representations*, 2023.
- [10] R. T. Q. Chen, X. Li, R. Grosse, D. Duvenaud, Isolating sources of disentanglement in vaes, in: *Proceedings of the 32nd International Conference on Neural Information Processing Systems*, 2018.
- [11] K. Hsu, W. Dorrell, J. C. R. Whittington, J. Wu, C. Finn, Disentanglement via latent quantization, in: *Neural Information Processing Systems*, 2023.
- [12] A. v. d. Oord, O. Vinyals, K. Kavukcuoglu, Neural discrete representation learning, in: *Advances in Neural Information Processing Systems*, 2017.
- [13] R. Rombach, A. Blattmann, D. Lorenz, P. Esser, B. Ommer, High-resolution image synthesis with latent diffusion models, *2022 IEEE/CVF Conference on Computer Vision and Pattern Recognition (CVPR) (2021)*.
- [14] A. Ramesh, M. Pavlov, G. Goh, S. Gray, C. Voss, A. Radford, M. Chen, I. Sutskever, Zero-shot text-to-image generation, *ArXiv abs/2102.12092 (2021)*.
- [15] H. Kim, A. Mnih, Disentangling by factorising, in: *International Conference on Machine Learning*, 2018.
- [16] X. Wang, H. Chen, S. Tang, Z. Wu, W. Zhu, Disentangled representation learning, *IEEE Transactions on Pattern Analysis and Machine Intelligence (2024)*.
- [17] I. Goodfellow, J. Pouget-Abadie, M. Mirza, B. Xu, D. Warde-Farley, S. Ozair, A. Courville, Y. Bengio, Generative adversarial nets, *Advances in neural information processing systems* 27 (2014).
- [18] J. Ho, A. Jain, P. Abbeel, Denoising diffusion probabilistic models, in: *Advances in Neural Information Processing Systems*, 2020.

- [19] I. Higgins, L. Matthey, A. Pal, C. Burgess, X. Glorot, M. Botvinick, S. Mohamed, A. Lerchner, β -VAE: learning basic visual concepts with a constrained variational framework, in: International Conference on Learning Representations, 2017.
- [20] F. Locatello, B. Poole, G. Raetsch, B. Schölkopf, O. Bachem, M. Tschannen, Weakly-supervised disentanglement without compromises, in: Proceedings of the 37th International Conference on Machine Learning, 2020.
- [21] C. Eastwood, J. von Kügelgen, L. Ericsson, D. Bouchacourt, P. Vincent, M. Ibrahim, B. Schölkopf, Self-supervised disentanglement by leveraging structure in data augmentations, in: Causal Representation Learning Workshop at NeurIPS 2023, 2023.
- [22] M. Yang, F. Liu, Z. Chen, X. Shen, J. Hao, J. Wang, Causalvae: Disentangled representation learning via neural structural causal models, in: Proceedings of the IEEE/CVF Conference on Computer Vision and Pattern Recognition (CVPR), 2021.
- [23] P. Esser, R. Rombach, B. Ommer, Taming transformers for high-resolution image synthesis, 2021 IEEE/CVF Conference on Computer Vision and Pattern Recognition (CVPR) (2020).
- [24] P. Dhariwal, H. Jun, C. Payne, J. W. Kim, A. Radford, I. Sutskever, Jukebox: A generative model for music, arXiv preprint arXiv:2005.00341 (2020).
- [25] L. Kaiser, S. Bengio, A. Roy, A. Vaswani, N. Parmar, J. Uszkoreit, N. Shazeer, Fast decoding in sequence models using discrete latent variables, in: Proceedings of the 35th International Conference on Machine Learning, 2018.
- [26] Y.-F. Wu, M. Lee, S. Ahn, Neural language of thought models, in: International Conference on Learning Representations, 2024.
- [27] G. Mercatali, A. Freitas, Disentangling generative factors in natural language with discrete variational autoencoders, in: The 2021 Conference on Empirical Methods in Natural Language Processing, 2021.
- [28] M.-A. Carbonneau, J. Zaïdi, J. Boilard, G. Gagnon, Measuring disentanglement: A review of metrics, IEEE Transactions on Neural Networks and Learning Systems 35 (2024) 8747–8761.
- [29] C. Eastwood, C. K. I. Williams, A framework for the quantitative evaluation of disentangled representations, in: International Conference on Learning Representations, 2018.
- [30] Y. Xu, S. Zhao, J. Song, R. Stewart, S. Ermon, A theory of usable information under computational constraints, in: International Conference on Learning Representations, 2020.

- [31] C. K. Sønderby, B. Poole, A. Mnih, Continuous relaxation training of discrete latent variable image models, Bayesian Deep Learning Workshop, NIPS 2017 (2017).
- [32] C. J. Maddison, A. Mnih, Y. W. Teh, The concrete distribution: A continuous relaxation of discrete random variables, in: International Conference on Learning Representations, 2017.
- [33] E. Jang, S. Gu, B. Poole, Categorical reparameterization with gumbel-softmax, in: International Conference on Learning Representations, 2017.
- [34] C. Burgess, H. Kim, 3D shapes dataset, 2018. URL: <https://github.com/deepmind/3dshapes-dataset/>.
- [35] W. Nie, High resolution disentanglement datasets, 2019. URL: <https://github.com/NVlabs/High-res-disentanglement-datasets>.
- [36] M. W. Gondal, M. Wuthrich, D. Miladinovic, F. Locatello, M. Breidt, V. Volchkov, J. Akpo, O. Bachem, B. Schölkopf, S. Bauer, On the transfer of inductive bias from simulation to the real world: a new disentanglement dataset, in: Advances in Neural Information Processing Systems, 2019.
- [37] W. Falcon, The PyTorch Lightning team, PyTorch Lightning, 2019. URL: <https://github.com/Lightning-AI/lightning>. doi:10.5281/zenodo.3828935.